# Thermal and Magnetic Field Switching in a Two-Step Hysteretic Mn(III) Spin Crossover Compound Coupled to Symmetry Breakings

Emiel Dobbelaar, Vibe B Jakobsen, Elzbieta Trzop, Minseong Lee, Shalinee Chikara, Xiaxin Ding, Helge G G Müller-Bunz, Kane Esien, Solveig Felton, Michael A Carpenter, et al.

# Thermal and Magnetic Field Switching in a Two-Step Hysteretic Mn(III) Spin Crossover Compound Coupled to Symmetry Breakings

Emiel Dobbelaar,*[a],† Vibe B. Jakobsen,[a],¤ Elzbieta Trzop,[b] Minseong Lee,[c] Shalinee Chikara,[c],‡ Xiaxin Ding,[c],§ Helge Müller-Bunz,[a] Kane Esien,[d],|| Solveig Felton,[d] Michael A. Carpenter,[e] Eric Collet,*[b] Grace G. Morgan*[a] and Vivien S. Zapf*[c]

[a] E. Dobbelaar, Dr. V. B. Jakobsen, Dr. H. Müller-Bunz, Prof. G. G. Morgan
School of Chemistry
University College Dublin
Science Centre Belfield, Dublin 4, Ireland
E-mail: grace.morgan@ucd.ie

[b] Dr. E. Trzop, Prof. E. Collet
University of Rennes
CNRS, IPR (Institut de Physique de Rennes)
UMR 6251, F-35000 Rennes, France
E-mail: eric.collet@univ-rennes1.fr

[c] Dr. S. Chikara, Dr. X. Ding, Dr. M. Lee, Dr. V. S. Zapf
National High Magnetic Field Laboratory
Los Alamos National Laboratory
Los Alamos, New Mexico 87545, United States
E-mail: vzapf@lanl.gov

[d] Dr. K. Esien, Dr. S. Felton
Centre for Nanostructured Media
School of Mathematics and Physics
Queen's University of Belfast
Belfast, BT7 1NN, Northern Ireland, United Kingdom

[e] Prof. M. A. Carpenter
Department of Earth Sciences,
University of Cambridge,
Downing Street, Cambridge CB2 3EQ, England, United Kingdom

Current addresses:

† Technische Universität Kaiserslautern, Fachbereich Chemie
ErwinSchrödinger-Str. 52-54, 67655, Kaiserslautern, Germany
¤ Nature Energy
Ørbækvej 260, 5220 Odense SØ, Denmark
‡ National High Magnetic Field Laboratory
Tallahassee, FL 32310, USA
§ City College of New York
New York, NY 10010
|| Cardiff University
Cardiff CF10 3AT, Wales, United Kingdom

Supporting information is given via a link at the end of the document.

A Mn(III) spin crossover complex with atypical two-step hysteretic thermal switching at 74 K and 84 K shows rich structural-magnetic interplay and magnetic field-induced spin state switching below 14 T with an onset below 5 T. The spin states, structures, and the nature of the phase transitions are elucidated via X-ray and magnetization measurements. An unusual intermediate phase containing four individual sites, where ¼ are in a pure low spin state, is observed. The splitting of equivalent sites in the high temperature phase into four inequivalent sites is due to a structural reorganization involving a primary and a secondary symmetry-breaking order parameter that induces a crystal system change from orthorhombic → monoclinic and a cell doubling. Further cooling leads to a reconstructive phase transition and a monoclinic low temperature phase with two inequivalent low spin sites. The coupling between the order parameters is identified in the framework of Landau theory.

## Introduction

A spin crossover (SCO) between low spin (LS) and high spin (HS) states of typically $3d^4$-$3d^7$ metal ions is a thermodynamic process that can induce large structural changes due to the change in 3d orbital occupancy and bond lengths.[1–4] The SCO corresponds to an evolution of the non-symmetry-breaking order parameter $q = \frac{N_{HS}-N_{LS}}{N_{HS}+N_{LS}}$, where $N_{HS}$ and $N_{LS}$ denote the number of sites in HS or LS states. Therefore, $q = +1$ in the full HS state and $q = -1$ in the fully LS state.[5,6] The elastic coupling between spin centres and the crystalline lattice results in a volume strain that can be weak, which would lead to a continuous SCO, or strong enough to drive a cooperative 1st (discontinuous) or 2nd order (continuous) phase transition.[7,8,9,10,11] In addition to single-step SCO, different types of stepwise thermally induced SCO between completely HS high temperature (HT) and LS low temperature (LT) phases have been reported, with an intermediate (INT) phase associated with a partial conversion from HS to LS states. Understanding and controlling such multi-stability is of prime importance and there are four main types of stepwise SCO discussed in the literature.[12] Type 1 corresponds to binuclear systems, with three molecular states (LS-LS, LS-HS or HS-HS) sequentially populated with increasing temperature.[13] Type 2 corresponds to SCO crystals containing asymmetric unit cells with two inequivalent molecular sites, forming sub-lattices 1 and 2, which switch sequentially with temperature.[14] Type 3 corresponds to mononuclear complexes exhibiting symmetry breaking on the step, due to the long-range ordering of HS and LS states over initially equivalent molecular sites.[15] Type 4 corresponds to a mixing of types 2 and 3, where one sub-lattice undergoes a two-step SCO and the other one a single step coupled to the one of the other sites.[16]

Various types of structural instabilities can lead to different symmetry-breaking (SB), with amplitudes that scale with the SB order parameter $\eta$, which also couples to volume change.[7,17] Thus, the nature of the SB can be very different, e.g. cell doubling/reconstructive ordering and crystal system changes (ferroelastic phase transitions) can both result from the loss/gain of symmetry operators between two phases with a group/subgroup relation.[7,12] The coupling of non-SB ($q$) and SB ($\eta$) order parameters to the volume strain results in the linear quadratic coupling $Dq\eta^2$ ($D$ being a measure of coupling strength),

as described in the framework of Landau theory.[5,18] In this case, a first-order, SB structural phase transition and a SCO can happen simultaneously. This allows for hysteretic switching and trapping of an excited spin state which sparks interest for applications such as memory effects.[3,6,19] The bi-quadratic coupling $Eq^2\eta^2$ can stabilize half conversion SCO (around $q = 0$).[5,16]

When the lattice change at the transition involves at least one phase with a polar space group, then the strong coupling between the structural order parameters and the SCO manifests as a strong coupling of the electric polarization and the magnetization, and thus, exhibits magnetoelectric coupling.[20,21,22,23,24] The coupling between the order parameters of the spin transition and the structural phase transition, in turn, influences the physical properties of the material.

SCO and its coupled properties[20,21,25] can be influenced and switched by external stimuli including temperature, light, pressure, electric and magnetic fields.[2,3,24,26] Compared to temperature, parameters such as electric and magnetic fields can allow for more rapid and/or improved control of material manipulation and are pursued for this reason.[25] Prominent research has featured light-induced excited spin state trapping (LIESST)[27] and magnetic field-induced spin state switching[28–31] as well as trapping (MIESST)[21,23,32] in compounds that show a thermal SCO. To date, magnetic field-induced SCO have mostly only been observed at high fields above 30 T, which limits the accessibility of these transitions.[10,24,33] Examples of compounds that show magnetic field-induced SCO behaviour below 14 T, which are accessible by typical superconducting magnets, are extremely rare.[21,23] In the few reported cases, the lower field-induced transitions can be observed just below the critical temperature of the cooperative SCO. A recently reported SCO material with a cooperative phase transition has proven to allow for hysteretic switching and trapping of a magnetic field-induced spin state at fields below 14 T at a SB, first-order phase transition boundary. Therefore a further investigation of similar materials seems worthwhile.[16,17] Investigation of the effects that influence and enable spin state switching at these more accessible fields should advance our understanding of the mechanisms of such phenomena and how they can be applied in device development.

## Results and Discussion

In this work, the discovery, synthesis, structural and magnetic properties of a new $Mn^{3+}$ SCO compound $[Mn^{III}sal_2(323)]ReO_4$ (**1**) ($sal_2(323)$ = 2,2'-(2,6,9,13-tetraazatetradeca-1,13-diene-1,14-diyl)diphenolate) (Scheme 1) are reported. As shown in Figure 1, the magnetic susceptibility ($\chi$) vs temperature ($T$), plotted as $\chi_M T$ vs $T$, for **1** exhibits stepwise SCO behaviour including two thermally hysteretic SCOs at 74 K and 84 K with widths of 6 and 1 K, respectively. This unusual behaviour results from the superposition of two types of symmetry breakings, which stabilizes the fractional conversion of ¾ of the LS sites to HS.

A sharp hysteretic transition in $\chi_M T$ is observed with critical temperatures of $T_{S1}\uparrow$ = 77 K and $T_{S1}\downarrow$ = 71 K determined from the peaks of $d(\chi_M T)/dT$ (Figure S2). A much smaller transition is observed centred at $T_{S2}$ = 84 K with a hysteresis width of about 1 K. The fact that $\chi_M T$ is approximately constant in $T$ and then changes sharply when crossing a narrow temperature range is consistent with a 1st order phase transition at a SCO from a lower to a higher spin state. At $T_{S1}$, $\chi_M T$ abruptly increases from 1.00 $cm^3 \cdot K \cdot mol^{-1}$ to 1.76 $cm^3 \cdot K \cdot mol^{-1}$ with a further abrupt increase at $T_{S2}$ to $\chi_M T$ = 1.87 $cm^3 \cdot K \cdot mol^{-1}$. The low temperature $\chi_M T$ value of 1.00 $cm^3 \cdot K \cdot mol^{-1}$ is consistent with the spin only value for a $Mn^{3+}$ ($d^4$) LS, S = 1 state. The stepwise thermal SCO gradually saturates from the high temperature end of the second thermal hysteresis to 2.35 $cm^3 \cdot K \cdot mol^{-1}$ at room temperature. This can be explained by temperature-induced population of the $m_L$ levels of both magnetic states following a Boltzmann distribution. The HS state has more accessible vibrational levels than the LS potential well, yielding a higher magnetization at high temperatures (equal population of the 8 $m_L$ levels would give $\chi_M T$ = 2.25 $cm^3 \cdot K \cdot mol^{-1}$). Second order effects may also include mixing of the ground state wavefunctions with energetically close wavefunctions of excited states and their orbital contributions. The consistency of the $\chi_M T$ value at high temperatures with a Boltzmann distribution implies no ordering of the S = 1 (LS) and S = 2 (HS) states in the high temperature phase. This is consistent with the observation of disorder of the counteranion in the HT phase (see 100 K structure, Figure S9) and with the gradual lattice changes above 84 K, which could be attributed to accommodating some spin state switching by elastic hydrogen bond length changes. A population of both HS and LS states at higher temperatures (100K, 250 K) is also consistent with the analysis of the bond lengths and in agreement with previous examples.[4] The value of 1.76 $cm^{-3} \cdot K \cdot mol^{-1}$ at the INT plateau at 80 K is consistent with a mixture of HS and LS states and can be understood by a structural analysis, which reveals that two of four individual cations in the asymmetric unit exhibit typical bond lengths for a HS and LS state, respectively, while the other two show intermediate bond lengths (HS*) with very similar HS concentrations (Table 1).

**Scheme 1.** Left: Structure of the most well-studied neutral $Mn^{3+}$ SCO complex Mn(taa). Middle: Structure of a $Mn^{3+}$ complex cation, $[Mn^{III}sal_2(323)]^+$, with an $N_4O_2^{2-}$ ligand donor set which has previously shown to promote SCO with

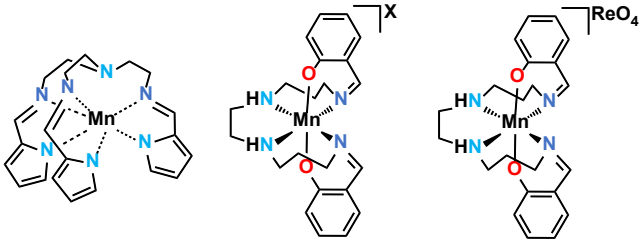


different charge balancing anions: $Cl^-$, $NO_3^-$, $AsF_6^-$, $PF_6^-$.[34,35]. Right: Structure of $[Mn^{III}sal_2(323)]ReO_4$, complex **1**.

Usually, hysteretic SCOs such as those observed in **1** result from lattice-mediated elastic coupling between individual molecules undergoing SCO and are often accompanied by structural phase transitions.[7,12,20,24] Hysteretic SCO in $d^4$ complexes remains rare [20,34–37] and here $ReO4^-$ was chosen as counterion in the $[Mn^{III}sal_2(323)]X$ SCO series with the aim of maximizing the intermolecular NH•••O interactions between the complex cations and anions, thereby encouraging a cooperative response (Scheme 1, Figure 2).[4,34,35]

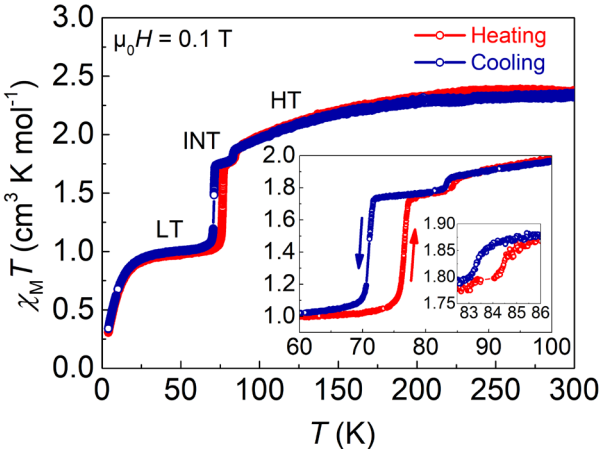


**Figure 1.** $\chi_M T$ vs $T$ measured at 0.1 T in a vibrating sample magnetometer (VSM) at 1 K/min on warming and cooling of a polycrystalline sample. A SCO occurs centered at 74 K with a hysteresis window of 6 K (larger inset). A second transition is observed at 84 K with a hysteresis window of ca. 1 K (smaller inset). $\chi_M T$ saturates at 2.35 $cm^3 \cdot K \cdot mol^{-1}$ at room temperatures. HT, INT and LT indicate the different phases identified by structural investigations (*vide infra*).

The structure of **1** was determined by single crystal X-ray diffraction at temperatures of 10 K, 80 K, 100 K, and 250 K, spanning the two SCO transitions centred at 74 K and 84 K, respectively. The unit cell contains either four (250 K, 100 K, 10 K) or eight (80 K) formula units of the complex cation $[Mn^{III}sal_2(323)]^+$ where the $Mn^{3+}$ cations occupy a distorted octahedral environment with two amine, two imine and two phenolate donors (Scheme 1, Figure 2), and are linked by the $ReO_4^-$ counteranions through H•••O bonds forming hydrogen bonded chains (Figures S8 – S13).

The hysteretic behaviour observed in Figure 1 is associated with a first-order phase transition, and thus cooperative in nature. In SCO materials such as this one, the spacing between magnetic ions and connection via organic linkers ensure that magnetic interactions are negligible. Instead, cooperativity results from coupling of the SCO to elastic lattice distortions. At the structural phase transition, this results in 1st order behaviour of the SCO and magnetic hysteresis. In particular, the hysteresis can be understood by considering the hydrogen bond interactions: (SCO-induced-) bond length changes in the first coordination sphere of one site directly affect the interactions and positions of the hydrogen-bonded $ReO_4^-$ anions and, thus, also the electronic situation of any other site that shares intermolecular interactions with this counteranion (see supporting information for more details). On a macroscopic level, these changes translate in the volume strain.

An elongation of the equatorial Mn-N bonds with increasing temperature is found as opposed to the axial Mn-O bonds (Table 1), which suggests the population of the $d_{x^2-y^2}$ orbital and axial compression. Therefore, the HS state of the metal centre is rationalized to be partially populated at 80 K and above. Additionally, the rather short bond lengths and low values of distortion parameters (Table 1 and S6) indicate that a mixture of S = 1 and S = 2 must be present at 80 K, 100 K and 250 K.

The cell parameters are enlarged by about 4 % between 10 K and 250 K (Table S1), inducing a significant volume strain that is most pronounced along the c-axis. Moreover, with respect to the parent high temperature-high symmetry phase, the first-order phase transitions that can also be followed by magnetometry measurements (Figure 1) are associated with two different symmetry changes on cooling: A ferroelastic phase transition from space group $P2_12_12_1$ to space group $P2_1$ accompanied by cell doubling around 84 K, and a reconstructive phase transition from $P2_1$ to a low temperature $P2_1$ space group with halving of the unit cell (Scheme 2). These discontinuous phase transitions result from a coupling between the structural symmetry change and the SCO.

The sequence of coupled spin and structural phase transitions from high temperature to low is: HS ($P2_12_12_1$) "HT phase"→ LS-HS-HS*-HS*, ($P2_1$) "INT phase" → LS-LS, ($P2_1$) "LT phase" (Figure 2). In the HT phase, the 4 molecules of the unit cell are equivalent and correspond to a single type of molecular site 1 (HS). Between 250 K and 100 K, there is a partial SCO, without symmetry change, revealed by magnetism (Figure 1), confirmed by the average contraction of the Mn-N bonds on site 1 (Table 1). The phase transition HT → INT consists of a first-order improper ferroelectric, improper ferroelastic phase transition as the lattice change from orthorhombic ($P2_12_12_1$) to monoclinic ($P2_1$) is also accompanied by a cell doubling along the a-direction. This is characterized by the appearance of Bragg peaks at Q-vector = 1/2a*, where a* is the reciprocal vector of the HT phase (Figure S14). The change of crystal system is evidenced by the appearance of (h00) peaks with h = 2n+1 and (00l) peaks with l = 2n+1, characteristic of the loss of the $2_1$ axis along a and c, as well as weak splitting of Bragg reflections in the h0l plane due to β-angle opening or closing from 90°. This splitting corresponds to the two types of ferroelastic domains that may form. The symmetry breaking results in the assignment of four independent $Mn^{3+}$ sites in two sublattices 1 and 2 in the asymmetric unit where three cations are assigned to HS (site 2B) or HS* states (sites 1A, 1B) and one is assigned to a pure LS state (site 2A), as confirmed by the bond-lengths shown in Table 1. The sites in sublattice 1 (1A and 1B) show very similar, intermediate bond lengths, indicative of a non-ordered mixture of HS and LS states, while the sites in sublattice 2 (2A and 2B) can clearly be assigned to LS/HS cations. This unusual scenario results from a preference in elastic interactions between adjacent cations that is only present in sublattice 2 (alternating HS-LS sites, "antiferroelastic" interactions).

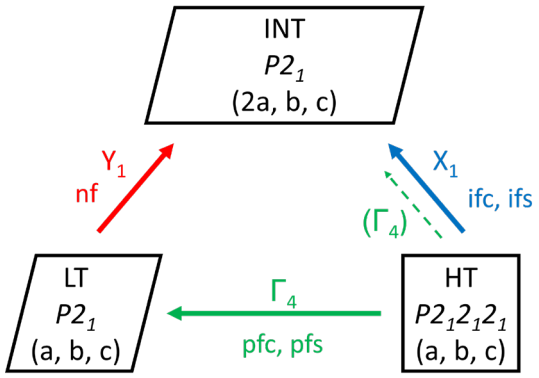


**Scheme 2.** Depiction of the group/subgroup relationships between the temperature dependent crystallographic phases with their respective irreps ($X_1$, $Y_1$, $\Gamma_4$).[38] i = improper, p = proper, fc = ferroelectric, fs = ferroelastic, nf = non-ferroic. See supporting information for supplementary discussion.

Below the INT → LT transition the system remains in the monoclinic $P2_1$ space group, but with the disappearance of the superstructure reflections at Q-vector = 1/2a* (measured at 10 K),

the cell doubling is lost and the periodicity along a corresponds to that of the HT phase. The crystal system remains monoclinic as the (h00) peaks with h = 2n+1 and (00l) peaks with l = 2n+1 are present in the LT phase (Figure S14). The two sublattices are retained and this leads to two independent $Mn^{3+}$ sites 1 and 2 in the LT phase where both are in the LS state (Table 1). As shown in Scheme 2, while the space group of the LT structure is *not* a subgroup of the space group of the INT one, the INT structure *is* a subgroup of the LT one. The INT → LT transition is, therefore, reconstructive. However, the LT structure is also a subgroup of the HT structure, thus there must be a possible transition HT → LT between ~84 and ~74 K which is metastable with respect to the stability field of the INT structure. This transition would be proper ferroelectric, proper ferroelastic but cannot be directly observed.

With respect to warming from the LT phase, the phase transition towards the INT phase corresponds to a cell doubling coupled to SCO as observed in many stepwise systems.

Both the transitions from HT to the INT and the LT phases are ferroelastic due to the change of crystal system from orthorhombic to monoclinic as the non-90º cell angle $\beta$ of the monoclinic structure represents the introduction of a symmetry breaking shear strain, $e_5$. The value of $e_5$ is given to good approximation by $\cos\beta$.[39] From the lattice parameter data given in Table 1, $e_5$ is -0.007 in the INT structure at 80 K and -0.001 in the LT structure at 10 K and thus rather small. The more important strain from the perspective of both energy changes and coupling between the symmetry breaking and SCO order parameters is associated with the volume reduction.

Already the partial SCO above 84 K induces a characteristic reduction in volume,[11] and gives rise to lattice distortions. As explained recently,[40] this can couple to the lattice strain associated with a symmetry breaking order parameter. Here, the coupling leads to the first order HT → INT transition at ~84 K.

The even larger volume change induced by the transitioning of ¾ of the present cations from HS or HS* to LS from the INT to the LT phase is coupled to a simultaneous, reconstructive phase transition to a higher symmetry which results in two independent $Mn^{3+}$ sites in the asymmetric unit of the LT phase.

To conclude this discussion about the group/subgroup relationships between the different phases, the space group of the parent HT structure $P2_12_12_1$ is considered as starting point (Scheme 2). For the $P2_12_12_1 \rightarrow P2_1$ LT transition the structural instability occurs at the $\Gamma$ point of the Brillouin zone. The symmetry-breaking order parameter has the symmetry of active representation $\Gamma_4$ and its amplitude $\eta_\Gamma$ measures the deviation from the orthorhombic lattice. For the $P2_1$ LT → $P2_1$ INT transition, the cell doubling instability corresponds to the symmetry-breaking order parameter $\eta_D$ which has the symmetry of active representation $Y_1$ (Scheme 2). For the $P2_12_12_1 \rightarrow P2_1$ INT transition, the two symmetry breakings occur simultaneously: the orthorhombic-monoclinic ferroelastic transition (order parameter $\eta_\Gamma$) makes sites 1 and 2 inequivalent and the cell doubling ($\eta_D$) makes sites A and B inequivalent. This order parameter for HT → INT has the symmetry of active representation $X_1$ (corresponding to $Y_1$ for the LT → INT symmetry breaking) and the ferroelastic distortion ($\eta_\Gamma$) is a secondary order parameter. Therefore, in the INT phase, the different spin states are distributed over the different molecular sites 1A (HS*), 1B (HS*), 2A (LS) and 2B (HS) (Table 1). This unusual symmetry breaking is responsible for the stabilization of a fraction of HS states on the step with 3 sites with significant HS concentrations (HS or HS*) and 1 pure LS site in the asymmetric unit.

Beyond the structural investigation, the magnetic field-induced switching of spin states in this compound was also examined. The anisotropic $d^4$ Jahn-Teller $Mn^{3+}$ ion has relatively small metal-ligand bond length changes at the SCO and a small energy gap between the two spin states as compared to other common SCO-materials.[4] Therefore, $Mn^{3+}$ SCO materials that exhibit thermal bistability are promising candidates to exhibit low magnetic field switching and MIESST effects.

**Table 1.** Selected bond lengths (Å) and structural parameters of **1** determined at 10 K, 80 K, 100 K and 250 K for all individual cations.[41]

| **Temperature** | **10 K** | | **80 K** | | | | **100 K** | **250 K** |
|---|---|---|---|---|---|---|---|---|
| **Space group** | **$P2_1$** | | **$P2_1$** | | | | **$P2_12_12_1$** | **$P2_12_12_1$** |
| **Cell Parameters** | | | | | | | | |
| **a** [Å] | 7.7029(2) | | 15.0635(3) | | | | 7.54017(15) | 7.7034(2) |
| **b** [Å] | 17.4473(5) | | 17.3425(3) | | | | 17.3374(3) | 17.3841(3) |
| **c** [Å] | 17.5523(5) | | 18.2478(3) | | | | 18.3276(3) | 18.3200(3) |
| **α** | 90° | | 90° | | | | 90° | 90° |
| **β** | 90.040(2)° | | 90.388(2)° | | | | 90° | 90° |
| **γ** | 90° | | 90° | | | | 90° | 90° |
| **Volume [Å³]** | 2358.94(11) | | 4766.92(15) | | | | 2395.91(7) | 2453.35(9) |
| **Z' [a]** | **2** | | **4** | | | | **1** | **1** |
| **Bond lengths** | Site 1 | Site 2 | Site 1A | Site 1B | Site 2A | Site 2B | Site 1 | Site 1 |

| | | | | | | | | |
|---|---|---|---|---|---|---|---|---|
| Mn-$O_{phen}$ | 1.878(12) | 1.872(12) | 1.878(8) | 1.875(8) | 1.875(9) | 1.860(9) | 1.875(4) | 1.879(4) |
| Mn-$O_{phen}$ | 1.884(12) | 1.871(11) | 1.874(8) | 1.878(9) | 1.885(9) | 1.869(9) | 1.872(4) | 1.868(4) |
| Mn-$N_{imine}$ | 1.991(14) | 2.000(15) | 2.051(11) | 2.040(11) | 1.986(10) | 2.065(9) | 2.055(5) | 2.104(5) |
| Mn-$N_{amine}$ | 2.079(13) | 2.045(15) | 2.145(11) | 2.107(12) | 2.061(11) | 2.237(10) | 2.153(4) | 2.189(5) |
| Mn-$N_{amine}$ | 2.047(14) | 2.062(14) | 2.148(10) | 2.129(11) | 2.066(10) | 2.211(10) | 2.163(5) | 2.213(5) |
| Mn-$N_{imine}$ | 1.995(14) | 1.975(13) | 2.057(11) | 2.020(12) | 1.991(10) | 2.097(10) | 2.049(4) | 2.067(5) |
| **Spin state** | LS | LS | HS* | HS* | LS | HS | HS* | HS |

[a] Z' is number of $Mn^{3+}$ sites in the asymmetric unit. Sites 1A and 1B at 80 K and Site 1 at 100 K display intermediate bond lengths and are thus assigned the HS* state. The HS* state does not represent a true HS state but an average spin state at this site with significant HS concentration. Distortion Parameters for the individual cations and additional details can be found in the supporting information (Table S6).

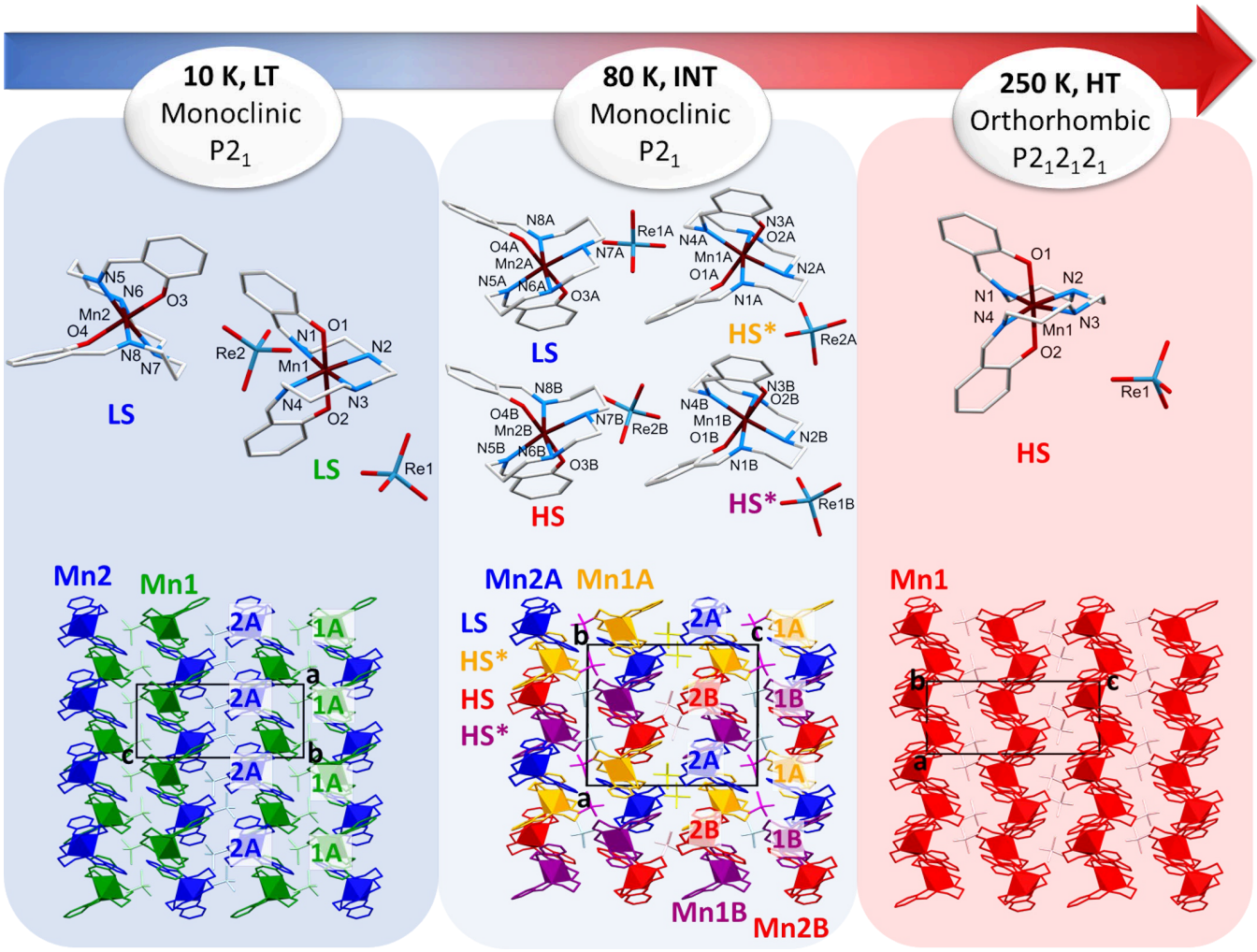


**Figure 2.** Perspective view as well as packing diagrams showing a simplification of symmetry breaking occurring for complex **1** measured at 10 K, 80 K and 250 K. The perspective view is shown with capped sticks and packing diagrams as capped sticks with the central Mn atom shown as a polyhedron. Hydrogen atoms are omitted for clarity. In the HT phase, all the $Mn^{3+}$ complex cation sites (1) are equivalent and HS. In the LT, there are two inequivalent LS sites 1 and 2 that represent the formation of two sublattices, shown in dark blue and dark green. In the INT phase, due to cell doubling with respect to the LT phase, the 1 and 2 sites split in inequivalent 1A-2A and 1B-2B sites. Red molecules represent $Mn^{3+}$ complex cations in a HS state, purple and yellow molecules represent individual sites that show a similar averaged mixed spin state HS*, blue and green molecules represent LS cations. The differing hydrogen bond interactions, short contacts and counteranion disorders in the structures obtained at various temperatures are illustrated and briefly discussed in the supporting information.

Magnetization (*M*) vs magnetic field (*H*) was measured in a Vibrating Sample Magnetometer (VSM) in a 14 T Physical Properties Measurement System (PPMS). A polycrystalline sample was measured for increasing and decreasing magnetic field and for different *T* between 74 and 76 K, shown in Figure 3. To rule out any artefacts, the sample was cooled to 60 K, warmed to the final measurement temperature, and thermalized for several hours before each measurement. Method limitations did cause an overshoot of up to 1 K upon warming before the final temperature was stabilized and may result in trapping of a higher spin state for 75 and 76 K prior to the exposure to a magnetic field (higher starting value for M/$\mu_0$H). This does, however, not influence the switching field $H_{S1}$(T) as is evident by a linear correlation of $H_{S1}$(T) vs T (Figure S3).

The *M* vs $\mu_0 H$ relation is approximately linear for magnetic fields in the downsweep and below 4 T in the upsweep. This quasi-linear behaviour is consistent with the Brillouin function for this temperature and magnetic field range as indicated in Figure 3. Smaller slopes below 74.5 K are consistent with a lower spin state and larger slopes above 74.5 K are consistent with a higher fraction of the HS state. Notably, there are field-induced transitions for the upsweep of the magnetic fields above 4 T on the ascending branch of the thermal hysteresis consistent with a partial magnetic field-induced crossover from a LS state to a higher spin state (Figure 3). These are hysteretic, such that once the higher spin state is achieved it is preserved on the downsweep, thus showing magnetic field-induced excited spin state trapping (MIESST). This is expected since the temperature is in the bistable regime of the SCO. The lowest field to induce a SCO to a higher state is observed at 75 K (centred at 9.9 T, onset below 5 T) in Figure 3. As would be expected from energetic considerations, the switching field $H_{S1}$(T) decreases with increasing temperature and can be observed when approaching the thermal transition temperature $T_{S1}$.[21]

The energetics that govern the magnetic field-induced phase transition involve overcoming the energy barrier that separates the LS from the HS phase at this 1st order phase transition. After this nucleation process occurs, the HS phase grows at the expense of the LS phase until the entire sample has transitioned. Applying a magnetic field lowers some $m_L$ levels of the HS state due to Zeeman splitting, making them thermally accessible and encouraging the nucleation and growth process. The switching is incomplete and suggests only a partial SCO as is consistent with energetic considerations as the thermally hysteretic SCO centred at 74 K is also incomplete. The gradual nature of the switching may be explained by an averaging of the different switching fields of differently oriented crystallites in the polycrystalline sample.[20,21,32] However, preliminary experiments on single crystals have shown gradual transitions as well and thus the gradual switching may have a different origin linked to the elastic interactions that are coupled to the SCO.

At this moment, mechanistic interpretations are speculative and require X-ray crystallographic investigations in high magnetic fields as a next step to elucidate if the field-induced HS states are equivalent to any of the temperature-induced phases.

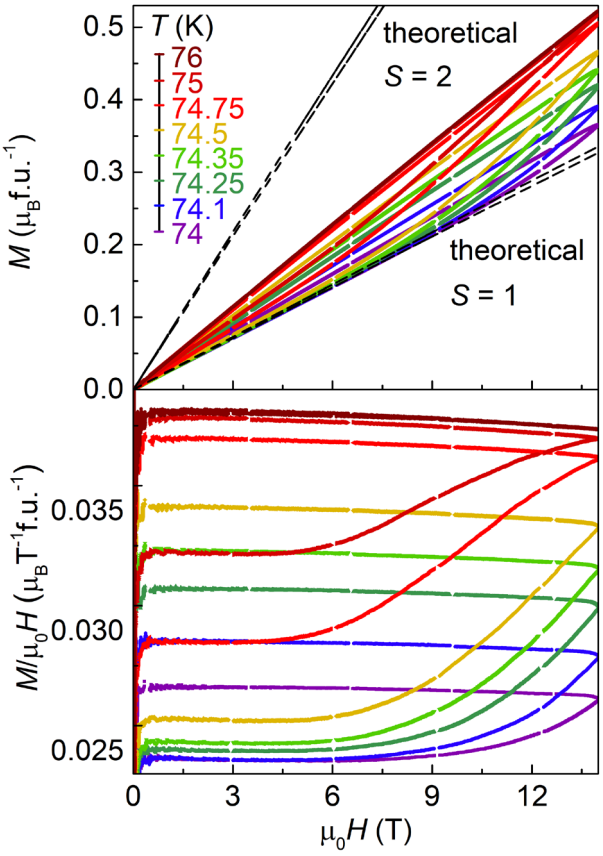


**Figure 3.** Top: Magnetization (M) vs magnetic field, ($\mu_0 H$) measured with a sweep rate of 50 Oe/s at different temperatures, *T* between 74 K and 76 K and *H* between 0 and 14 T of a polycrystalline sample. Dashed lines indicate the theoretical Brillouin functions for the *S* = 2 and the *S* = 1 states for both 74 K and 76 K. Bottom: Experimental data plotted as M/$\mu_0 H$ vs $\mu_0 H$ to show the magnetic field-induced transitions more clearly.

## Conclusion

In conclusion, a newly synthesized $Mn^{3+}$ complex shows a stepwise spin conversion coupled to two symmetry changes: a ferroelastic orthorhombic → monoclinic distortion and a cell doubling. These occur simultaneously during the HT → INT phase transition, which stabilizes a fraction of HS states on the step. Only few examples of stepwise spin transitions[8] have been reported for $Mn^{3+}$ compounds[32,36,42], this being one of the first examples of a $Mn^{3+}$ SCO-compound that shows more than one thermally-hysteretic SCO and consequently two different (but related) couplings of SCO and SB first-order phase transitions.[32] The unusual behaviour results from the structural reorganization of the INT phase involving a primary and a secondary symmetry-breaking order parameter, splitting sites that are equivalent in the HT phase into four: sites 1 and 2 are due to the monoclinic → orthorhombic distortion and sites A and B are due to cell doubling. This reorganization results in a ¾ fraction with HS or HS* sites (A1, A2 and B1) and a ¼ fraction with a LS site (B2). The INT → LT phase transition involves a symmetry increase on cooling and is first order (reconstructive). The LT high symmetry structure is stabilised by coupling of SCO with a different symmetry breaking order parameter.

Magnetic field-induced spin state trapping (MIESST) at a relatively low field can be observed in a 2 K range close to the ascending branch of the wider hysteresis. The effect can be observed with DC fields below 14 T with an onset of the magnetic field-induced switching below 5 T at 75 K (centred at 9.9 T at 50 Oe/s). To date, investigations of SCO as a function of magnetic field are much rarer than those induced by temperature, light or pressure.[28–32] When SCO materials are exposed to applied magnetic fields, those fields are usually in the range of pulsed magnetic fields, 30 T DC fields or higher. Thus, it is unusual and significant that the reported compound shows SCO effects in magnetic fields starting even below 5 T.

The unusually rich interplay between SCO, structural ordering and SB gives rise to two transitions with significant thermal and magnetic hysteresis, with two different types of symmetry breakings and cross-coupling of properties underscoring the potential of the spin switchable Jahn-Teller $Mn^{3+}$ ion for multifunctional behaviour.

## Acknowledgements

The NHMFL experimental facility at LANL is funded by the U.S. National Science Foundation through Cooperative Grant No. DMR-1157490, the State of Florida, and the U.S. Department of Energy. VSZ and ML were funded by the Center for Molecular Magnetic Quantum Materials (M2QM), an Energy Frontier Research Center funded by the U.S. Department of Energy, Office of Science, Basic Energy Sciences under Award DE SC0019330. G.G.M. thanks Science Foundation Ireland (SFI) for support via Frontiers for the Future Award (19/FFP/6909). V.B.J. was supported by the Irish Research Council GOIPG/2016/73 fellowship, Augustinus Fonden (Grant No. 18-0338), Oticon Fonden (Grant No. 17-3813), Reinholdt W. Jorck og Hustrus Fond (Grant No. 18-JI-0573), P.A. Fiskers Fond, A.P. Møller og Hustru Chastine Mc-Kinney Møllers Fond til almene Formaal, and Christian og Ottilia Brorsons Rejselegat for yngre videnskabsmænd og-kvinder. ET and EC were funded by Agence Nationale de la Recherche, ANR-19-CE30-0004 ELECTROPHONE, ANR-19-CE07-0027 SMAC. E.C. thanks the Fondation Rennes 1 for support. SC was funded by the LANL Laboratory-Directed Research and Development program.

**Keywords:** ferroelastic materials • manganese • spin crossover • structural phase transition • magnetic properties

## References

[1] K. Senthil Kumar, M. Ruben, *Coord. Chem. Rev.* **2017**, *346*, 176.
[2] P. Gütlich, Y. Garcia, H. A. Goodwin, *Chem. Soc. Rev.* **2000**, *29*, 419.
[3] M. A. Halcrow, *Chem. Soc. Rev.* **2008**, *37*, 278.
[4] J. Olguín, *Coord. Chem. Rev.* **2020**, *407*, 213148.
[5] G. Azzolina, R. Bertoni, E. Collet, *J. Appl. Phys.* **2021**, *129*, 85106.
[6] H. Watanabe, K. Tanaka, N. Bréfuel, H. Cailleau, J.-F. Létard, S. Ravy, P. Fertey, M. Nishino, S. Miyashita, E. Collet, *Phys. Rev. B* **2016**, *93*, 014419.
[7] M. Shatruk, H. Phan, B. A. Chrisostomo, A. Suleimenova, *Coord. Chem. Rev.* **2015**, *289-290*, 62.
[8] S. Vela, H. Paulsen, *Inorg. Chem.* **2018**, *57*, 9478.
[9] a) H. Spiering, K. Boukheddaden, J. Linares, F. Varret, *Phys. Rev. B* **2004**, *70,* 184106; b) A. Hauser, P. Guetlich, H. Spiering, *Inorg. Chem.* **1986**, *25*, 4245.
[10] A. Bousseksou, G. Molnár, L. Salmon, W. Nicolazzi, *Chem. Soc. Rev.* **2011**, *40*, 3313.
[11] H. E. Mason, W. Li, M. A. Carpenter, M. L. Hamilton, J. A. K. Howard, H. A. Sparkes, *New J. Chem.* **2016**, *40*, 2466.
[12] E. Collet, P. Guionneau, *C. R. Chim.* **2018**, *21*, 1133.
[13] E. Trzop, M. Buron-Le Cointe, H. Cailleau, L. Toupet, G. Molnar, A. Bousseksou, A. B. Gaspar, J. A. Real, E. Collet, *J. Appl. Crystallogr.* **2007**, *40*, 158.
[14] a) B. Weber, C. Carbonera, C. Desplances, J.-F. Létard, *Eur. J. Inorg. Chem.* **2008**, 1589; b) Y. Garcia, O. Kahn, L. Rabardel, B. Chansou, L. Salmon, J. P. Tuchagues, *Inorg. Chem.* **1999**, *38*, 4663; c) G. S. Matouzenko, J.-F. Létard, S. Lecocq, A. Bousseksou, L. Capes, L. Salmon, M. Perrin, O. Kahn, A. Collet, *Eur. J. Inorg. Chem.* **2001**, 2935; d) M. M. Ndiaye, S. Pillet, E.-E. Bendeif, M. Marchivie, G. Chastanet, K. Boukheddaden, S. Triki, *Eur. J. Inorg. Chem.* **2018**, 305; e) A. T. Brennan, K. A. Zenere, C. J. Kepert, J. K. Clegg, S. M. Neville, *Inorg. Chem.* **2021**, *60*, 3871.
[15] a) M. Griffin, S. Shakespeare, H. J. Shepherd, C. J. Harding, J.-F. Létard, C. Desplanches, A. E. Goeta, J. A. K. Howard, A. K. Powell, V. Mereacre et al., *Angew. Chem. Int. Ed.* **2011**, *50*, 896, *Angew. Chem.* **2011**, *123*, 926; b) Z.-Y. Li, J.-W. Dai, Y. Shiota, K. Yoshizawa, S. Kanegawa, O. Sato, *Chem. Eur. J.* **2013**, *19*, 12948; c) B. J. C. Vieira, J. T. Coutinho, I. C. Santos, L. C. J. Pereira, J. C. Waerenborgh, V. da Gama, *Inorg. Chem.* **2013**, *52*, 3845; d) D. J. Harding, W. Phonsri, P. Harding, K. S. Murray, B. Moubaraki, G. N. L. Jameson, *Dalton Trans.* **2015**, *44*, 15079; e) M. Paez-Espejo, M. Sy, K. Boukheddaden, *J. Am. Chem. Soc.* **2016**, *138*, 3202; f) D. Boinnard, A. Bousseksou, A. Dworkin, J. M. Savariault, F. Varret, J. P. Tuchagues, *Inorg. Chem.* **1994**, *33*, 271; g) D. Chernyshov, M. Hostettler, K. W. Törnroos, H.-B. Bürgi, *Angew. Chem. Int. Ed.* **2003**, *42*, 3825; h) N. Huby, L. Guérin, E. Collet, L. Toupet, J.-C. Ameline, H. Cailleau, T. Roisnel, T. Tayagaki, K. Tanaka, *Phys. Rev. B* **2004**, *69*, 020101(R); i) D. L. Reger, C. A. Little, V. G. Young, M. Pink, *Inorg. Chem.* **2001**, *40*, 2870; j) V. A. Money, C. Carbonera, J. Elhaïk, M. A. Halcrow, J. A. K. Howard, J.-F. Létard, *Chem. Eur. J.* **2007**, *13*, 5503; k) J. Luan, J. Zhou, Z. Liu, B. Zhu, H. Wang, X. Bao, W. Liu, M.-L. Tong, G. Peng, H. Peng et al., *Inorg. Chem.* **2015**, *54*, 5145; l) M. Yamada, H. Hagiwara, H. Torigoe, N. Matsumoto, M. Kojima, F. Dahan, J.-P. Tuchagues, N. Re, S. Iijima, *Chem. Eur. J.* **2006**, *12*, 4536; m) T. Sato, K. Nishi, S. Iijima, M. Kojima, N. Matsumoto, *Inorg. Chem.* **2009**, *48*, 7211; n) E. Collet, H. Watanabe, N. Bréfuel, L. Palatinus, L. Roudaut, L. Toupet, K. Tanaka, J.-P. Tuchagues, P. Fertey, S. Ravy et al., *Phys. Rev. Lett.* **2012**, *109*, 257206; o) S. Bonnet, M. A. Siegler, J. S. Costa, G. Molnár, A. Bousseksou, A. L. Spek, P. Gamez, J. Reedijk, *Chem. Commun.* **2008**, 5619; p) J. E. Clements, J. R. Price, S. M. Neville, C. J. Kepert, *Angew. Chem. Int. Ed.* **2016**, *55*, 15105, *Angew. Chem.* **2016**, 128,15329.
[16] K. D. Murnaghan, C. Carbonera, L. Toupet, M. Griffin, M. M. Dîrtu, C. Desplanches, Y. Garcia, E. Collet, J.-F. Létard, G. G. Morgan, *Chem. Eur. J.* **2014**, *20*, 5613.
[17] E. K. Salje, *Phase Transitions in Ferroelastic and Co-elastic Crystals*, Cambridge University Press, **2011**.
[18] a) G. Azzolina, R. Bertoni, C. Ecolivet, H. Tokoro, S. Ohkoshi, E. Collet, *Phys. Rev. B* **2020**, *102*, 134104; b) Z. Zhang, J. Koppensteiner, W. Schranz, D. Prabhakaran, M. A. Carpenter, *J. Phys. Condens. Matter* **2011**, *23*, 145401.
[19] a) M. Buron-Le Cointe, J. Hébert, C. Baldé, N. Moisan, L. Toupet, P. Guionneau, J. F. Létard, E. Freysz, H. Cailleau, E. Collet, *Phys. Rev. B* **2012**, *85*, 064114; b) R. Bertoni, M. Lorenc, A. Tissot, M.-L. Boillot, E. Collet, *Coord. Chem. Rev.* **2015**, *282-283*, 66.

[20] V. B. Jakobsen, E. Trzop, L. C. Gavin, E. Dobbelaar, S. Chikara, X. Ding, K. Esien, H. Müller-Bunz, S. Felton, V. S. Zapf et al., *Angew. Chem. Int. Ed.* **2020**, *59*, 13305, *Angew. Chem.* **2020**, 132, 13407.
[21] V. B. Jakobsen, S. Chikara, J.-X. Yu, E. Dobbelaar, C. T. Kelly, X. Ding, F. Weickert, E. Trzop, E. Collet, H.-P. Cheng et al., *Inorg. Chem.* **2021**, *60*, 6167.
[22] a) M. Nakano, G. Matsubayashi, T. Matsuo, *Phys. Rev. B* **2002**, *66*, 212412; b) C. Lefter, R. Tan, J. Dugay, S. Tricard, G. Molnár, L. Salmon, J. Carrey, W. Nicolazzi, A. Rotaru, A. Bousseksou, *Chem. Phys. Lett.* **2016**, *644*, 138; c) W. Zhang, R. Alonso-Mori, U. Bergmann, C. Bressler, M. Chollet, A. Galler, W. Gawelda, R. G. Hadt, R. W. Hartsock, T. Kroll et al., *Nature* **2014**, *509*, 345.
[23] Y. Otsuki, S. Kimura, S. Awaji, M. Nakano, *AIP Adv.* **2019**, *9*, 85219.
[24] S. Chikara, J. Gu, X.-G. Zhang, H.-P. Cheng, N. Smythe, J. Singleton, B. Scott, E. Krenkel, J. Eckert, V. S. Zapf, *Nat. Commun.* **2019**, *10*, 4043.
[25] O. Sato, *Nat. Chem.* **2016**, *8*, 644.
[26] a) P. Gütlich, H. A. Goodwin, *Spin Crossover in Transition Metal Compounds I*, Springer Berlin Heidelberg, Berlin, Heidelberg, **2004**; b) P. Gütlich, H. Goodwin, *Spin Crossover in Transition Metal Compounds II*, Springer Berlin Heidelberg, Berlin, Heidelberg, **2004**; c) P. Gütlich, A. B. Gaspar, Y. Garcia, *Beilstein J. Org. Chem* **2013**, *9*, 342; d) E. Tailleur, M. Marchivie, J.-P. Itié, P. Rosa, N. Daro, P. Guionneau, *Chem. Eur. J.* **2018**, *24*, 14495; e) N. Negre, M. Goiran, A. Bousseksou, J. Haasnoot, K. Boukheddaden, S. Askenazy, F. Varret, *Synth. Met.* **2000**, *115*, 289; f) P. Gütlich, A. Hauser, H. Spiering, *Angew. Chem. Int. Ed.* **1994**, *33*, 2024, *Angew. Chem.* **1994**, 106, 2109; g) S. Decurtins, P. Gütlich, C. P. Köhler, H. Spiering, A. Hauser, *Chem. Phys. Lett.* **1984**, *105*, 1; h) Y. Garcia, O. Kahn, J.-P. Ader, A. Buzdin, Y. Meurdesoif, M. Guillot, *Physics Letters A* **2000**, *271*, 145.
[27] a) C. Bressler, C. Milne, V.-T. Pham, A. Elnahhas, R. M. van der Veen, W. Gawelda, S. Johnson, P. Beaud, D. Grolimund, M. Kaiser et al., *Science* **2009**, *323*, 489; b) G. Auböck, M. Chergui, *Nat. Chem.* **2015**, *7*, 629.
[28] Y. Qi, E. W. Müller, H. Spiering, P. Gütlich, *Chem. Phys. Lett.* **1983**, *101*, 503.
[29] J. Lejay, A. G. M. Jansen, P. Wyder, W. Bronger, and W. Kläui, *Phys. Rev. B,* **1991**, *43*, 8196.
[30] S. Kimura, Y. Narumi, K. Kindo, M. Nakano, G. Matsubayashi, *Phys. Rev. B* **2005**, *72*, 064448.
[31] M. M. Altarawneh, G.-W. Chern, N. Harrison, C. D. Batista, A. Uchida, M. Jaime, D. G. Rickel, S. A. Crooker, C. H. Mielke, J. B. Betts et al., *Phys. Rev. B* **2012**, *109*, 37201.
[32] V. J. Jakobsen, E. Trzop, E. Dobbelaar, L. C. Gavin, S. Chikara, X. Ding, M. Lee, K. Esien, H. Müller-Bunz, S. Felton et al., *J. Am. Chem. Soc.* **2021**, *accepted*.
[33] A. Bousseksou, K. Boukheddaden, M. Goiran, C. Consejo, M.-L. Boillot, J.-P. Tuchagues, *Phys. Rev. B* **2002**, *65*, 172412.
[34] S. Wang, Y.-J. Li, F.-F. Ju, W.-T. Xu, K. Kagesawa, Y.-H. Li, M. Yamashita, W. Huang, *Dalton trans.* **2017**, *46*, 11063.
[35] P. N. Martinho, B. Gildea, M. M. Harris, T. Lemma, A. D. Naik, H. Müller-Bunz, T. E. Keyes, Y. Garcia, G. G. Morgan, *Angew. Chem. Int. Ed.* **2012**, *51*, 12597, *Angew. Chem.* **2012**, 124, 12765.
[36] A. J. Fitzpatrick, E. Trzop, E. Trzop, H. Müller-Bunz, M. M. Dîrtu, Y. Garcia, E. Collet, G. G. Morgan, *Chem. Commun.* **2015**, *51*, 17540.
[37] A. V. Kazakova, A. V. Tiunova, D. V. Korchagin, G. V. Shilov, E. B. Yagubskii, V. N. Zverev, S. C. Yang, J.-Y. Lin, J.-F. Lee, O. V. Maximova et al., *Chem. Eur. J.* **2019**, *25*, 10204.
[38] D. M. Hatch, H.T. Stokes, *Isotropy Subgroups Of The 230 Crystallographic Space Groups*, World Scientific, **1989**.
[39] M. A. Carpenter, E. K. Salje, A. Graeme-Barber, *Eur. J. Mineral.* **1998**, *10*, 621.
[40] E. Collet, G. Azzolina, *Phys. Rev. Mater.* **2021**, *5*, 044401.
[41] The crystal data collection and refinement parameters details for this paper can be obtained free of charge via www.ccdc.cam.ac.uk/conts/retrieving.html (or from the Cambridge Crystallographic Data Centre, 12 Union Road, Cambridge CB2 1EZ, UK; fax: (+44) 1223-336-033; or deposit@ccdc.ca.ac.uk) respectively via the CCDC 20780992, 20780993, 20780994, 20780995.
[42] a) S. Ghosh, S. Bagchi, M. Das, S. Kamilya, A. Mondal, *Dalton trans.* **2020**, *49*, 14776; b) S. Ghosh, S. Bagchi, S. Kamilya, A. Mondal, *Dalton trans.* **2021**, *50*, 4634.

**Entry for the Table of Contents**

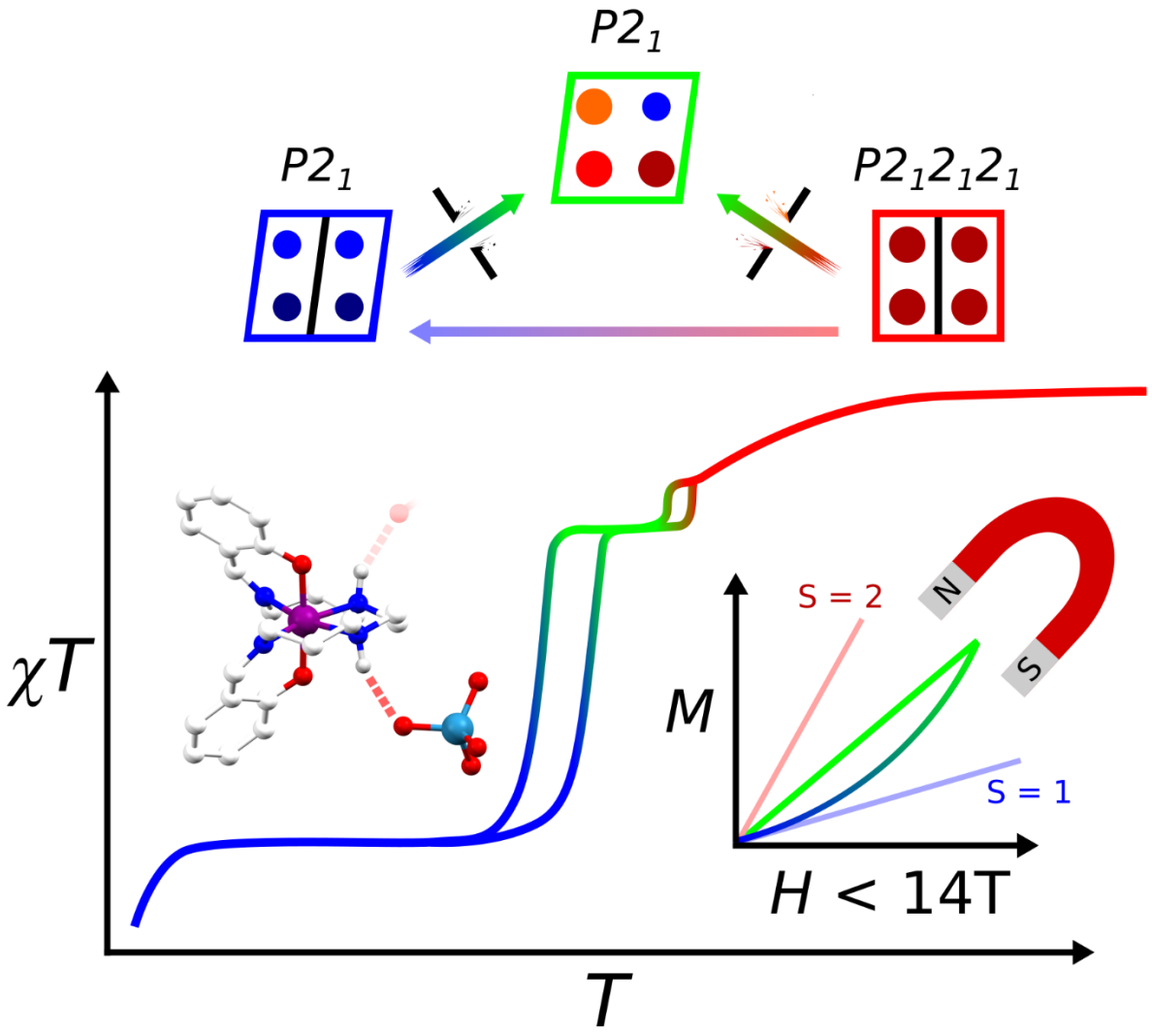


A new Mn(III) compound shows stepwise spin crossover (SCO) with two thermal hystereses coupled to symmetry breaking phase transitions. The superposition of two types of symmetry breakings leads to a rich interplay between structural and magnetic properties and stabilizes an unusual intermediate phase with four independent Mn(III) sites. Magnetic field-induced spin state switching at unprecedently low DC fields (onset <5 T) is observed.

Institute and/or researcher Twitter usernames: @emieldobb, @rx_collet